Journal of Building Engineering 78 (2023) 107372

Contents lists available at ScienceDirect

Journal of Building Engineering

journal homepage: www.elsevier.com/locate/jobe

Full length article

Small-scale experiments on the operational performance of a lightweight thermally active building system

G.P. Lydon [a,b,c,*], A. Schlueter [a,b]

[a] Architecture and Building Systems, ETH Zurich, Stefano-Franscini-Platz 1, Switzerland
[b] NCCR Digital Fabrication, ETH Zurich, Stefano-Franscini-Platz 1, Switzerland
[c] Department of Architecture and Technology, Norwegian University of Science and Technology, NTNU, Trondheim, Norway

ARTICLE INFO

Keywords:
Thermally activated building system (TABS)
Integrated design
Multifunctional elements
Embodied energy
Operational energy
Lifecycle energy design

ABSTRACT

Thermally active building systems (TABS), which are integrated with the structure of a building, provide a robust approach for utilising renewable energy. However, reinforced concrete, where TABS are typically placed, is responsible for a significant proportion of initial embodied energy and related greenhouse gas emissions. Therefore, combining lightweight structural elements and thermal systems reduces initial embodied energy usage while retaining the active material's thermal storage and heat transport benefits. The present experimental work explores the operational performance of a prototype of a lightweight TABS at ceiling level. A small-scale climate chamber was constructed and equipped to evaluate the prototype in the key operating modes. The study investigated the relationship between the supply temperature of the lightweight TABS and the climate chamber's internal air temperature for active heating, active cooling and natural ventilation modes. The experiments compared the reaction time in active heating mode for a range of supply temperatures. In addition, we examined the dynamic characteristics of the thermal mass of the lightweight TABS in passive natural ventilation mode and passive cooling mode in the presence of an internal thermal load. The results provide insights into the dynamic performance in operation. In heating mode, we identified the time lag between the radiant surface achieving a steady state and the conditioned air reaching its target temperature. This feature emphasises the significance of refining control strategies when designing comfortable environments with low-temperature heating systems at ceiling level. Further, we highlighted the importance of balancing decisions on minimising embodied energy with the suitability of the selected material to leverage renewable energy sources. The experimental data can be used for validating high-resolution numerical models, which support the development of multifunctional elements with renewable energy sources for building heating and cooling.

1. Introduction

Thermally active building systems (TABS) offer an attractive path to incorporate renewable energy into the built environment [1]. Combining a geothermal heat pump with TABS is seen as the ideal technique for harnessing low exergy approaches [2] for interior conditioning, which takes advantage of a lower lift operation of heat pumps and a reduction of distribution losses [3]. TABS are classified as radiant systems because radiation is the primary heat transfer mode. Compared to all-air systems, radiant systems have been shown to provide a superior level of thermal comfort with significant energy savings [4]. Further, designers can add passive

* Corresponding author at: Department of Architecture and Technology, Norwegian University of Science and Technology, NTNU, Trondheim, Norway.
E-mail address: gplydon@gmail.com (G.P. Lydon).

https://doi.org/10.1016/j.jobe.2023.107372
Received 19 May 2023; Received in revised form 27 June 2023; Accepted 14 July 2023
Available online 9 August 2023

Nomenclature

τ_{63}	Time constant (h)
$\dot{V}$	Volumetric flow rate, (m^3/s)
Δ T	Temperature difference (K)
σ	Stefan–Boltzmann constant (W m/K^4)
A	Opening area (m^2)
C_d	Discharge coefficient
g	Gravitational acceleration (m/s^2)
GHG	Greenhouse gas
h	Opening height (m)
HSE	Heat storage efficiency (%)
HTE	Heat transfer efficiency (%)
HVAC	Heating, ventilation, and air conditioning
Q	Ventilation flow rate, (m^3/s)
q	Heat transfer rate (W)
$q_{conduction}$	Heat transfer rate by conduction (W)
$q_{convection}$	Heat transfer rate by convection (W)
$q_{radiation}$	Heat transfer rate by radiation (W)
RTD	Resistance temperature detector
$T_{ceiling}$	Temperature of ceiling surface (°C)
T_I	Temperature of climate chamber air (°C)
T_{pipe}	Temperature of TABS pipe (°C)
T_{room}	Temperature of room air (°C)
$T_{surface}$	Temperature of room surface (°C)
TABS	Thermally active building system
U	Thermal transmittance (W m^2/K)
XPS	Extruded polystyrene

methods (e.g. natural ventilation) by utilising the thermal mass or the heat storage features of the concrete materials [5], which enables the shifting of heating and cooling loads to match the availability of the renewable sources [6]. TABS are typically integrated with structural concrete elements. However, the cement sector is the third largest industrial energy user, accounting for around 7% of worldwide greenhouse gas (GHG) emissions [7]. The use of reinforced concrete in buildings is responsible for a considerable proportion of initial embodied energy and related GHG emissions [8]. In addition, the slow thermal response times of TABS in heavyweight concrete structures cause problems for effective control during the operational phase [9].

To mitigate the outlined problems, the use of concrete can be restricted to components with high functionality [10]. With this strategy, a lightweight structural element is integrated with a TABS and forms the floor or the ceiling of a room [11], and the remainder of the structure (e.g. walls and columns) uses lower embodied energy materials (e.g. wood). The structural element realises a significant reduction of concrete material volume of up to 70% [12] due to the optimisation of the geometry to a vaulted shape where the dominant loads are mainly compressive [13]. Further, this approach contributes to circular design by moving the steel reinforcement to a tension tie at the floor boundary, which improves the efficiency of decommissioning at the end-of-life phase.

This multifunctional design approach [14], which is driven by advances in digital fabrication [15], minimises volumes of a high embodied energy material while maintaining the material's influence on the building's operational performance. Therefore, the lightweight TABS concept (Fig. 1) refers to the overall thermal mass in the room and not just the active component. Extracting the maximum functionality from a selected material can potentially improve the total building lifecycle energy [16].

When thin concrete panels are used for TABS, there are efficiency and performance benefits due to an improvement in reaction time and a reduction in thermal losses to the external environment [17]. However, the approach requires expertise on the material's influence on structures and a detailed understanding of the HVAC performance characteristics on the operational side. This point is important for a multifunctional component because optimising the structure by reducing material in a specific region could have a negative impact on the thermal performance of the HVAC systems [16].

The main objective of this paper is to provide insights into the key operational modes of TABS in lightweight concrete structures based on measurements from small-scale experiments. The work assesses the thermal characteristics of a ceiling-level TABS embedded in a thin concrete element. The remainder of the climate chamber (e.g. floor and walls) is composed of wooden materials. The dynamic behaviour in heating and cooling modes for various supply temperatures is examined. The same experimental setup also evaluates natural ventilation and thermal mass mechanisms. These experiments provide an understanding of the relationship between the temperatures of the thermally active surface with room air and non-active surfaces. The results measure the reaction

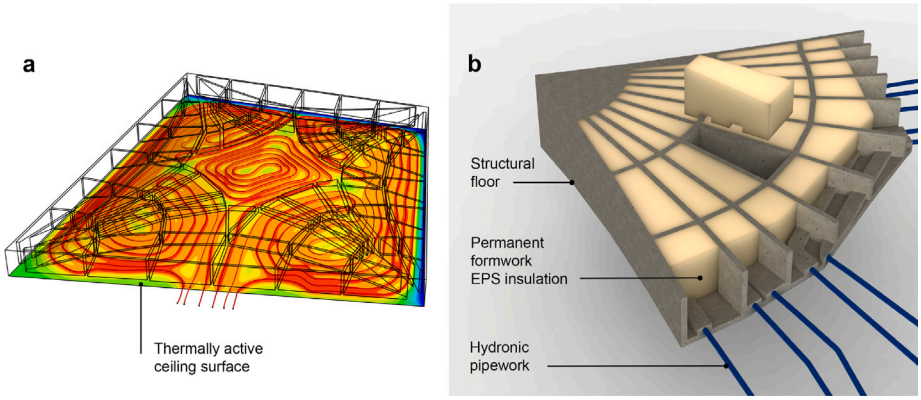

Fig. 1. Design phase models of a lightweight TABS for a structural floor. (a) High-resolution model of the thermally active ceiling surface in heating mode showing the temperature contours at the ceiling surface. (b) Conceptual model of the assembly of the multifunctional floor system.

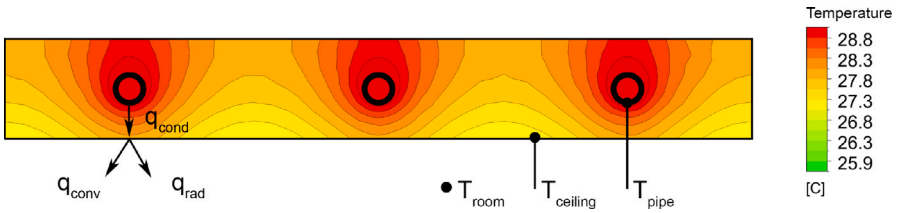

Fig. 2. The energy balance at the ceiling surface for a lightweight TABS with the heat flux and reference temperature.

time in attaining operational surface temperature, which is improved compared to typical heavyweight systems due to the thinness of the concrete panel. However, the heating mode shows a time lag from reaching the operational surface temperature to the target temperatures for room air and the non-active surfaces. This issue relates to the physics of low-temperature heating systems at ceiling level, which can be overcome using appropriate control strategies.

A detailed description of the experimental apparatus and an online data set of the measurements are provided. The research findings can be used to validate simulation methods for the product development of lightweight TABS (Fig. 1a) and support the development of digital twins for thermal systems.

The paper is organised as follows: to emphasise the contribution of the research, review and background information of relevant topics is outlined in Section 2. Section 3 discusses the methodology for the experimental study. The results of each experiment are highlighted in Section 4. Section 5 discusses the implications of the research outcomes and an outline of future work. Finally, the main conclusions are summarised in Section 6.

2. Review, background and research questions

2.1. Heat transfer of radiant systems

Heat transfer coefficients are critical parameters for the development of HVAC systems. For radiant systems with a renewable energy source, a detailed understanding of convective and radiant heat flux is particularly important (Fig. 2 and Eq. (1)). This requirement is due to a supply water temperature, typically 23 to 35 °C in heating mode, that is near to room temperature, and the dependence on large internal surfaces for radiant heat emission [18].

Convective and radiant coefficients do not have the same reference temperature. The radiant coefficient is based on the surface-to-surface heat transfer within the zone, and the convective coefficient (h_{conv}) uses room air temperature (T_{room}) as a reference. Due to the different reference temperatures, a total heat transfer coefficient calculation uses operative temperature as a reference [19]. For illustrative purposes, Eq. (2) describes the energy balance [20,21] at the ceiling surface for a TABS in a simplified form.

$$q_{conduction} = q_{convection} + q_{radiation} \tag{1}$$

$$U(T_{pipe} - T_{ceiling}) = h_{conv}(T_{ceiling} - T_{room}) + \sum_{n=1}^{j} \sigma \epsilon_c F_{c\rightarrow j}(T_{ceiling}^4 - T_{surface(j)}^4) \tag{2}$$

Where U is thermal transmittance (W/m^2 K), T_{pipe} is the temperature of the TABS pipe (K), $T_{ceiling}$ is the temperature of the ceiling surface (K), $T_{surface}$ is the temperature of the other room surfaces (K), σ is the Stefan–Boltzmann constant (W m/K^4), ϵ_c is the emissivity of the ceiling surface and F_c is the view factor of the ceiling to other surfaces.

Table 1
Total heat transfer coefficients (W/m^2 K) for radiant systems with source references depending on conditioning mode and room surface.

Component	Total heat transfer coefficient (W/m^2 K)	
	Heating	Cooling
Floor	11 [22]	7 [27]
Ceiling	6 [27]	13.2 [28]
Walls	8 [27]	8 [27]

For a temperature range between 15 °C and 35 °C, the radiant coefficient can be taken as 5.5 W/m^2 K [22]. The associated convective component is dependent on the location of the emitting surface (e.g. floor, ceiling or wall) and the mode of operation (e.g. heating or cooling). See Table 1 for a summary of typical values for total heat transfer coefficients for radiant systems. For a detailed discussion on heat transfer coefficients for radiant heating and cooling systems see the review by Shinoda et al. [23].

One of the advantages of radiant systems at ceiling level is the higher cooling capacity (~100 W/m^2) in comparison to walls (~70 W/m^2) and floors (~40 W/m^2) [24]. Based on the expected increase in cooling degree days in Central Europe by the end of the century [25], this approach could be an effective method of preparing for the impact of climate change in new buildings and through the vertical extension of renovated buildings [26].

2.2. Experimental studies on radiant systems

A brief review of recent research highlights relevant studies and the benefits of experimental investigations for a range of pertinent topics relating to radiant systems.

Causone et al. [28] conducted experiments in a room-scale climate chamber. Heated cylinders and losses by chilled surfaces represented internal heat gains. The primary outcome was the determination of heat transfer coefficients and a detailed methodology for calculating reference temperatures. A further study tested the cooling capacity of a radiant ceiling panel and emphasised the importance of reference temperatures when estimating heat transfer coefficients separately for product development [29].

Laboratory measurements with climate chambers and a hot box were used to test an innovative radiant wall system [30]. Hydronic pipework was combined with insulating bricks to form a wall heating and cooling system. The results showed a fast thermal response time in operation. In addition to the experimental measurements, a full-scale room was simulated using computational fluid dynamics (CFD) to quantify thermal output and comfort. This strategy of combining experimental and simulated methods provided a deep understanding of the dynamic systems of the product. Venk et al. investigated mixed convection over a thermally active wall in a specially built climate chamber [31]. These articles demonstrated the advantages of vertical TABS, which is a valuable concept for the retrofit of buildings with a carbon-based heat source.

An understanding of thermal response is an important design driver for the operational performance of radiant systems [32]. The time constant (τ_{63}) indicator [33] is related to the time taken to reach 63% of the steady state of an observed variable (e.g. thermal output or surface temperature of a TABS panel). Other response times can also be used depending on the investigation (e.g. τ_{80} and τ_{95}). Heat transfer efficiency (HTE) is used to characterise the efficiency of heat transfer between the embedded pipes and the radiant surface [34]. Heat storage efficiency (HSE) indicates the heat flux distribution on the radiant surface [32]. HSE can distinguish between the quantity of heat stored in the structure and heat transferred to the room, which is a useful indicator when developing TABS with complex geometry. This group of indicators can support the design of innovative radiant systems during the product development phase.

The interplay of hanging sound absorbers and TABS was considered to determine the effect on thermal conditions [35]. For an 80% acoustic absorber coverage, the drop in cooling performance was 36%. These findings are important for planning of ceiling-level TABS in an office setting.

Nagler et al. conducted empirical validation and code-to-code comparisons of several building simulation tools using a test chamber with a heavyweight TABS [36]. The TRNSYS model developed by Koschenz and Lehmann [37] performed well compared to experiments. For example, the comparison of simulated and measured water return temperature, which is an essential parameter for the operational control of TABS in non-residential buildings.

The dynamic thermal response of a radiant floor system to simulated direct sunlight was explored in a study [38]. The findings indicate a 4 °C local overheating for 11.5 h after the solar load was switched off. Therefore, designers should consider the influence of solar loading for TABS control strategies in buildings with high window-to-wall ratios.

Experiments were conducted to evaluate the use of phase change materials to increase the thermal mass of a radiant system [39]. The results demonstrated that the added thermal mass offered enough heat storage capacity to shift cooling demand to off-peak periods. This active technique has the potential to assist large-scale building renovations.

Room-scale experiments were used to support the product development of a combined TABS and ventilation strategy [40,41]. The results quantified the advantages of coupling ceiling-level TABS with diffuse ventilation. Krusaa et al. examined the coupling of diffuse ventilation, and a radiant ceiling panel [42]. The test was conducted using a small-scale experiment of the perforated panel, and the dimensions were sized for similitude. The results showed an increase of 20% in the total heat transfer coefficient for the cooling mode.

An experiment was performed to investigate radiative heat transmission in a full-scale room with displacement ventilation and a local heat source [20]. A set of 30 thermocouples were affixed to a vertical pole and used to measure air temperature. The surface temperature in the room was recorded using 22 thermocouples distributed across the walls and ceiling. Several tests were conducted to determine the effect of changing the heat load, wall emissivity, inlet flow rate, and inlet temperature. The results provided vertical air temperature profiles on the room under various boundary conditions. The experiment's high quantity of data points offered a valuable opportunity for validating high-resolution numerical models, which Gilani et al. implemented [21]. The experimental data were used for validation and sensitivity analysis for displacement ventilation using CFD methods. The work provided comprehensive information on the grid resolution, turbulence models, and discretisation methods needed to analyse stratified indoor air with a heat source.

There is a lack of detailed experimental studies at the ceiling level on the thermal performance of the lightweight TABS approach to facilitate product development using numerical modelling. This work can support the validation of modelling methods. In particular, the interaction between the active thermal mass and the other materials in the room. This work aims to close the identified research gap.

2.3. Project background

The development of the lightweight TABS has been advanced using simulation and experimental methods. The four main research stages for the overall project are listed below:

1. High-resolution modelling [14,17]
2. Small-scale experiments
3. White-box modelling [16]
4. Full-scale demonstrator.

In previous work, we detailed the energy analysis of incorporating lightweight TABS throughout the design phase on a building and district-scale [14,17]. There was a focus on using a simulation framework to identify the thermal loads and to match this demand with the available renewable energy sources. We also discussed a white-box modelling technique utilised by the energy domain to facilitate the creation of a digital twin [16]. This approach supported operational phase issues such as the interaction of the lightweight TABS with other HVAC devices and control strategies. The present paper documents the application of a small-scale experiment used during the project's development phase.

2.4. Research questions and target audience

The research aimed to provide thermal measurements of the lightweight TABS under varied operating conditions. We specified a small-scale experiment with sufficient data points to capture the initial, operating and boundary conditions. The research questions that prompted this study are outlined below:

1. What is the relationship between a lightweight TABS supply temperature and the climate chamber's internal air temperature for active heating, active cooling and natural ventilation modes?
2. What is the reaction time for the lightweight TABS in active heating mode for a range of supply temperatures?
3. How does the temperature of the thermal mass (lightweight TABS) change in passive natural ventilation mode?
4. How does the temperature of the thermal mass (lightweight TABS) change with the presence of an internal thermal load?

The outcomes of the studies can support researchers developing TABS in low thermal mass buildings. The data relating to the system's dynamic thermal behaviour under various conditions can assist in validating high-resolution numerical models. These validated models can estimate key performance indicators (e.g. heat and cooling capacity) of innovative systems with complex geometry during the development phase. An important advantage of the study is that all operating modes are included in the experiment plan. The experimental data supports future independent research by the scientific community, which can contribute to an improved understanding of lightweight TABS. Furthermore, the data sets of the experimental cases are made available for future independent research by the scientific community, which can contribute to an improved understanding of lightweight TABS.

3. Methodology

3.1. Experiment description

The small-scale experiment is implemented using a climate chamber with an internal volume of 1.21 m^3. The climate chamber is located in a test room (8 m × 5 m × 2.2 m) at an underground level, which minimised significant thermal disturbances (e.g. solar loads, equipment loads) and provided stable thermal conditions for the duration of the experiments. The climate chamber is fitted with a lightweight TABS, located at ceiling level with an exposed concrete surface area of 1.12 m^2. The small-scale experiment's key geometrical features (e.g. concrete panel thickness and materials) are related to a planned full-scale investigation. The setup is completed with a thermal hydronic system, a sensor network and a data acquisition device (Fig. 3).

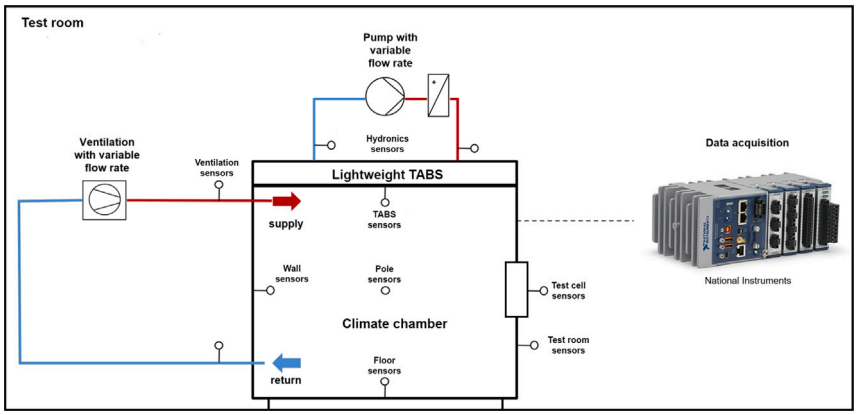

Fig. 3. Schematic of the small-scale experiment setup with sensor groups.

Fig. 4. Constructing the concrete panel. (a) Preparing the formwork and reinforcement for the lightweight concrete panel. (b) Placing and finishing the concrete layer. (c) Securing the TABS pipework to the concrete panel. (d) Applying the concrete cover to the TABS pipework and pipe surface temperature sensor.

The results from the small-scale experiment should be scaled for the chamber size when compared to full-scale rooms [42]. In particular, for the present work, the impact of natural convective heat transfer at an internal surface should be considered [43]. In addition, Awdi and Hatton [44] noted considerable differences in the convective heat transfer coefficient between a small-scale chamber and a full-scale room. This effect is due to the differences in temperature stratification, resulting in lower air movement near the ceiling in the chamber. Therefore, the pole group of sensors has been added to monitor temperature stratification. A schematic of the overall system and the sensor groups are provided in Fig. 3. The ventilation systems and the test cell are not used for these experiments. A brief description of the construction of the experimental setup is provided in this section.

3.2. TABS panel

The lightweight concrete panel has a thickness of 35 mm, and it is reinforced with a carbon textile mesh (Solidian Grid Q85/85-CCE-21) (Fig. 4a), which was placed on the central plane of the panel. There is a 200 mm overlap of the mesh reinforcement directly under the location of the TABS pipe (Fig. 4a). The concrete mix has the typical characteristics of lightweight structures with complex geometry (Fig. 4b) requiring high workability levels (e.g. the maximum aggregate size was limited to 5 mm). The thermal properties of the concrete materials were measured with an ISOMET 2114 [45], which is a hand-held measuring instrument for direct estimation of heat transfer properties. The results for the concrete materials are available in Table 5.

The TABS pipe is an Uponor Velta PE-Xa with a 20 mm outside diameter and a wall thickness of 2.3 mm. The pipe was securely attached to the concrete panel with adhesive and brackets at a spacing of 200 mm (Fig. 4c), and a layer of concrete cover was

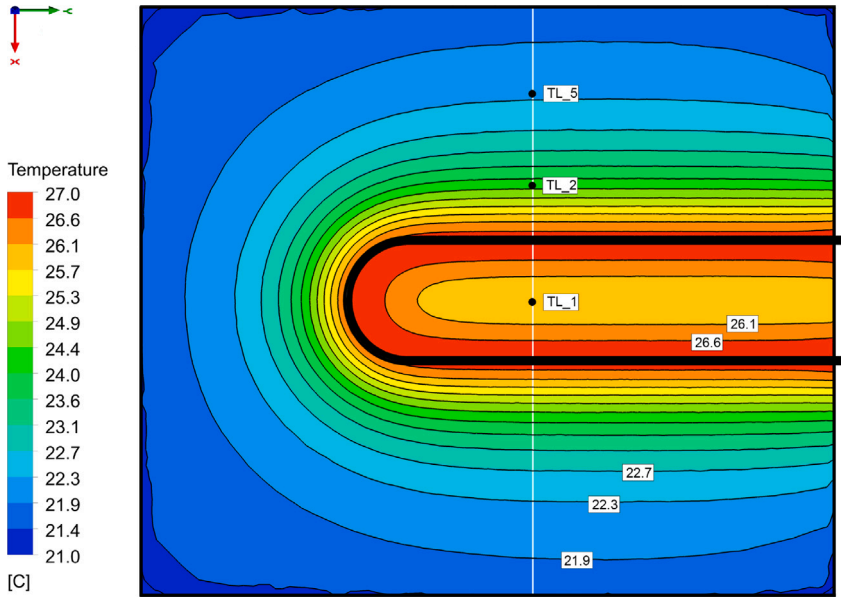

Fig. 5. Preliminary CFD study — Results from Case 1. Lower surface temperature contours. Location of the TABS pipework is superimposed in black. The white line is the location for plotting the temperature profile. The locations of the temperature sensors on the lower surface (TL_1), (TL_2) and (TL_5) are shown.

added to ensure adequate thermal contact with the concrete panel (Fig. 4d). To minimise thermal edge effects at the connection between the panel and the walls, the panel was sized to provide an adequate distance from the pipe to the panel boundary. This sizing was based on a preliminary CFD study, which was completed before the experiment was constructed. The CFD model was limited to the panel and the connecting wall geometry. The air volume inside the climate chamber was not modelled, and a heat transfer coefficient of 6 W/m^2 K was applied at the lower surface of the panel. The simulation was completed in ANSYS Fluent, and an outline of the model setup can be found in previous work [16]. Fig. 5 shows the temperature contours of the lower surface of the TABS panel. The position of the TABS pipework is superimposed in black. It can be seen that the thermally active region is mainly at the centre of the panel. There is thermal interaction between the panel and the wall where the TABS pipework enters the panel. This feature should be adequately planned in the model when preparing a high-resolution CFD study of the full climate chamber.

After the experiments were completed, the CFD model was run with the initial and boundary conditions of Case 1 (e.g. water supply temperature of 30.8 °C). The results for this case can be seen in Fig. 6 with the measured values from the sensors (TL_1, TL_2 and TL_5) on the lower surface of the panel and the sensors (TU_1, and TU_2) on the upper surface of the panel.

3.3. Climate chamber construction

The construction of the climate chamber was completed with plywood, and the insulation layer was formed with expanded polystyrene (XPS) insulation (Fig. 7a). This configuration represents the lightweight TABS concept as the main thermal mass is contained in the concrete ceiling, and the remainder of the form (e.g. walls and floor) are constructed with low thermal mass materials (e.g. wood). When the chamber form was completed, the TABS panel was placed and insulated (Fig. 7b). The layer thickness and material properties of the chamber can be found in Table 5. The dimensions of the internal surfaces of the chamber and images of the construction are outlined from Figs. 8 to 12.

3.4. Hydronic system

A thermal hydronic system was constructed with a supply temperature range of 20 °C to 40 °C and a variable flow rate. This setup consisted of a variable flow pump, a hydronic manifold and an electric water heater with temperature control (Siemens DE2124628M). The water flow rate was measured with an ultrasonic volumetric flow device (Bellimo EV015R+BAC), which has an accuracy of ±2% (of 25...100% V'nom) at 20 °C. The supply and return temperature was measured with resistance temperature detectors (RTDs) of type PT1000 (Bellimo), which were immersed in the water flow. The hydronic system was attached to the side of the climate chamber and connected to the TABS pipework (Fig. 7c).

3.5. Sensor groups and data acquisition

The sensor groups (Fig. 7d) were installed and connected to a National Instruments cDAQ-9133 Controller for data acquisition and control (Fig. 7d). The temperature sensors are PT100 or PT1000, depending on the location. A data point list with sensor group details is provided in Table 6.

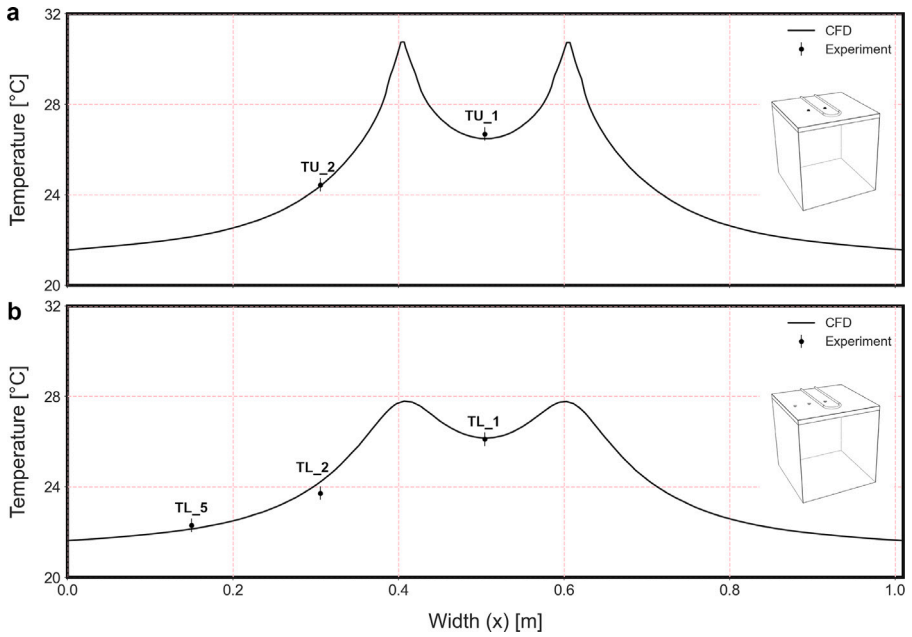

Fig. 6. Preliminary CFD study — Results from Case 1. (a) Comparison of the temperature of the upper surface of the TABS panel by CFD simulation and experiment (TU_1 and TU_2) results. (b) Comparison of the temperature of the lower surface of the TABS panel by CFD simulation and experiment (TL_1, TL_2 and TL_5) results.

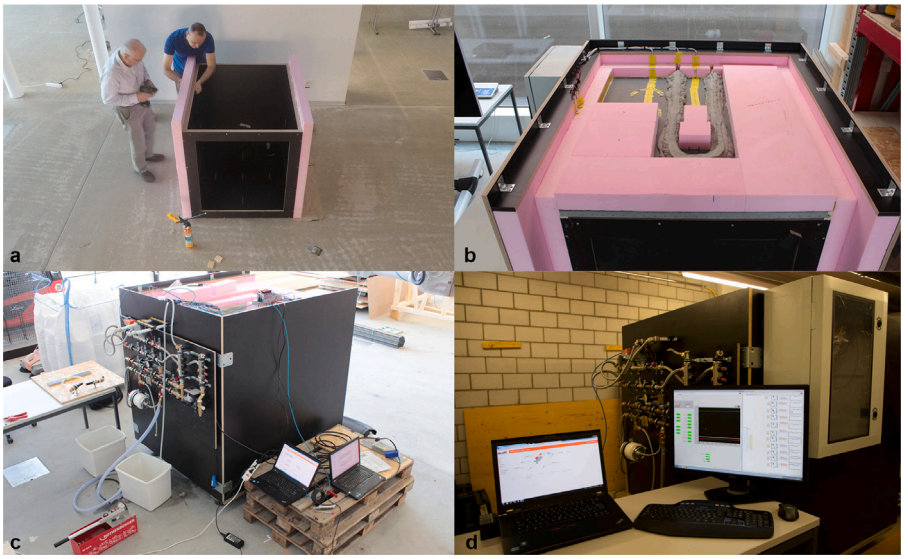

Fig. 7. Constructing the climate chamber. (a) Applying the XPS insulation layers. (b) Installing and insulating the concrete panel. (c) Testing the hydronic system. (d) Completing the data acquisition setup.

3.6. Experimental plan

The experimental strategy is to generate data on the dynamic thermal characteristics of the lightweight TABS. The experiments were divided into four groups related to the operational modes:

1. TABS heating (active)
2. TABS cooling (active)
3. Natural ventilation (passive)
4. Passive cooling.

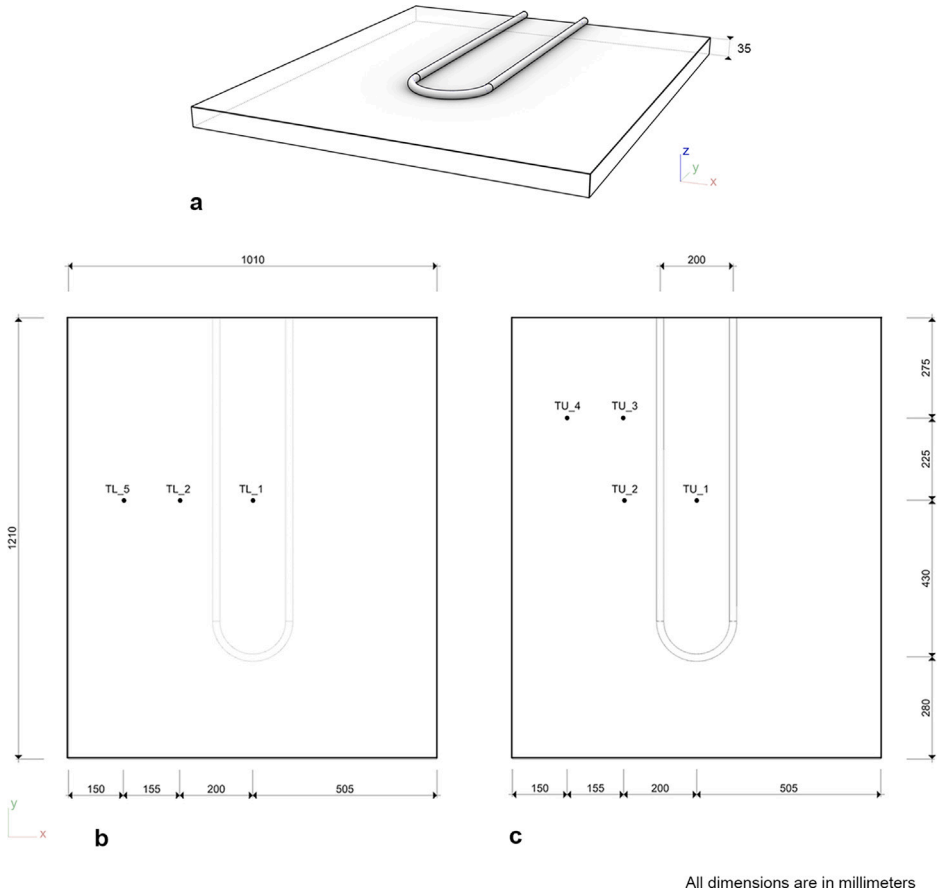

Fig. 8. Schematic of positions the TABS sensors group. (a) Isometric view of the TABS panel. (b) Internal view of the TABS panel. (c) Top view of the TABS panel.

The first three experiment groups (Table 2) were conducted in sequence (e.g. Case 1, 4 and 7) from TABS heating to TABS cooling to natural ventilation (Fig. 20). Before the start of each sequence, the majority of temperature sensors had a steady state temperature of less than 15 °C. For active heating, the water heater was set to the TABS supply temperature and the water circulation pump to the TABS flow rate. The chamber door was closed for the duration of the experiment. For active cooling, the water heater was turned off, and the water was circulated through a heat exchanger that was exposed to the test room air. The circulation pump was switched off for natural ventilation mode, and the chamber door was opened. The overall duration of a sequence was 120 h.

The passive cooling experiment (Table 3) was run from steady-state conditions where the equipment had a temperature of less than 20 °C. The hydronic system was switched off, and the chamber door was closed. An electric heater with an integrated fan was placed inside the chamber, which provided an internal heat load. The heater was located near the back wall of the climate chamber to avoid direct interaction between the heater airflow and the chamber sensors. The fan was set to the maximum flow rate level for the duration of the experiments, which ensured adequate mixing of air within the climate chamber. A schematic of the location and the airflow direction is provided in Fig. 13.

The parameters of each experiment group are presented in Tables 2 and 3. Overview plots of all of the experiment groups are provided in Appendix B. The raw experimental dataset with a time resolution of five seconds and the experiment geometry are available on an online data repository.

4. Results

This section summarises the main results and outcomes for the four research questions.

4.1. Internal chamber temperature and operating mode

We examined the relationship between a lightweight TABS supply temperature and the climate chamber's internal air temperature for active heating, active cooling and natural ventilation modes. The experimental conditions for each of the 9 cases are presented in Table 2.

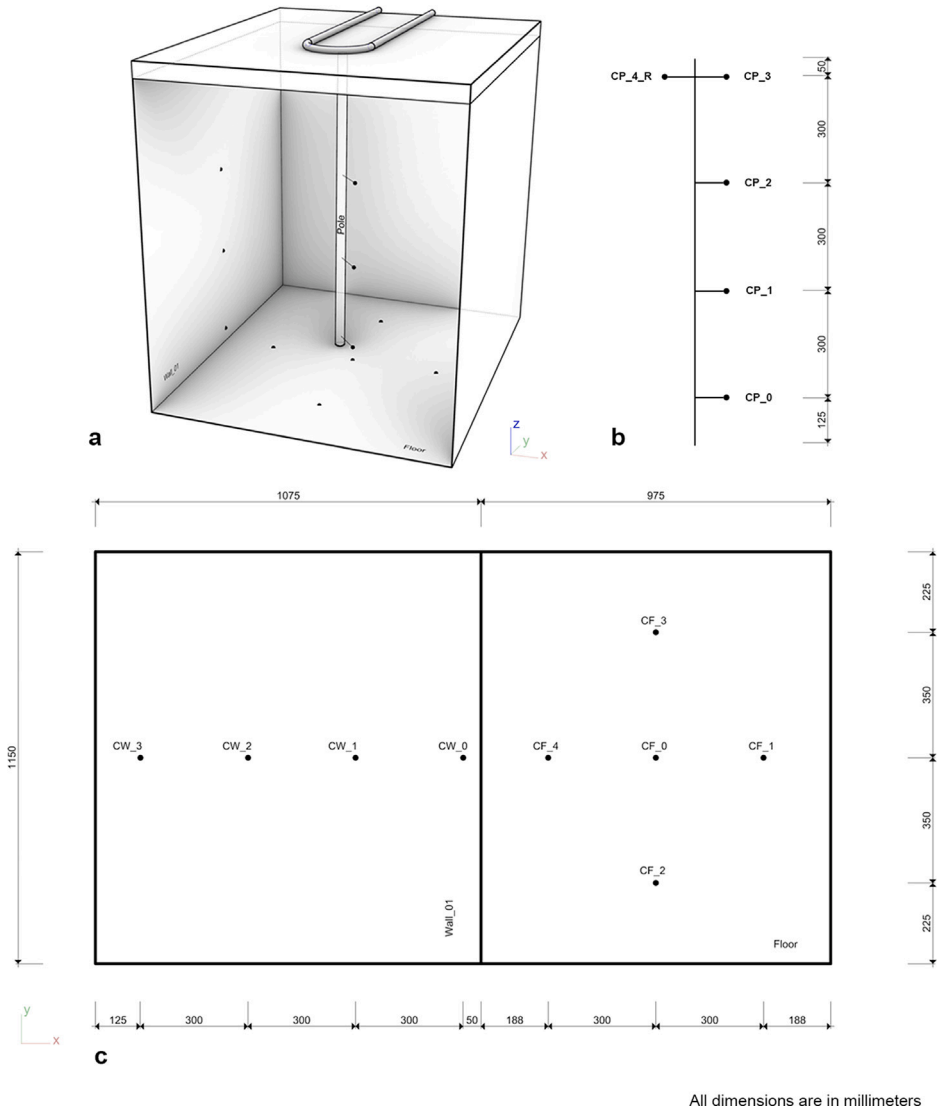

Fig. 9. Schematic of positions the wall, floor and pole sensor groups. (a) Isometric view of the climate chamber. (b) Schematic of the pole sensor group (c) Developed view of a wall and floor of the climate chamber.

Table 2
Experiment plan I.

Experiment		TABS	TABS	TABS	Chamber	Duration
Case	Type	pump state	flow rate [l/min]	supply temperature [°C]	door state	[h]
1	TABS heating	On	4	30	Closed	72
2	TABS heating	On	4	35	Closed	72
3	TABS heating	On	4	40	Closed	72
4	TABS cooling	On	4	20	Closed	24
5	TABS cooling	On	4	20	Closed	24
6	TABS cooling	On	4	20	Closed	24
7	Natural ventilation	Off	-	-	Open	24
8	Natural ventilation	Off	-	-	Open	24
9	Natural ventilation	Off	-	-	Open	24

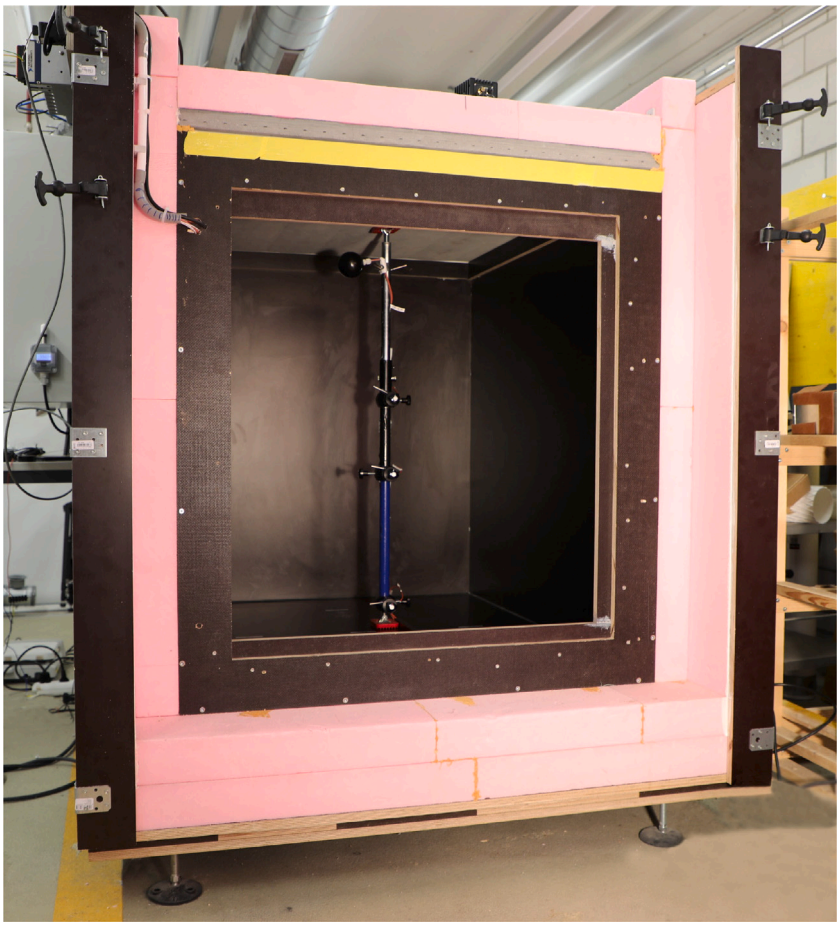

Fig. 10. Inside the climate chamber showing the TABS panel and the pole sensor group with the door open.

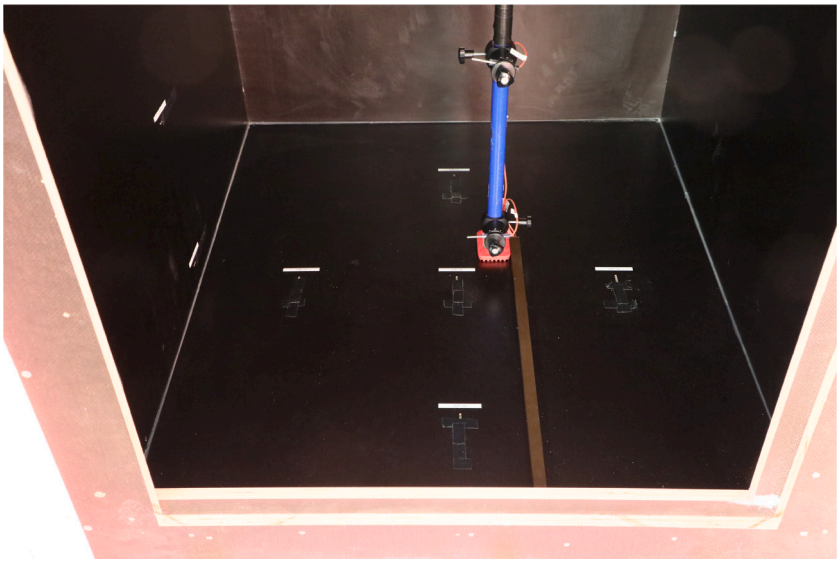

Fig. 11. Inside the climate chamber showing the floor sensor group.

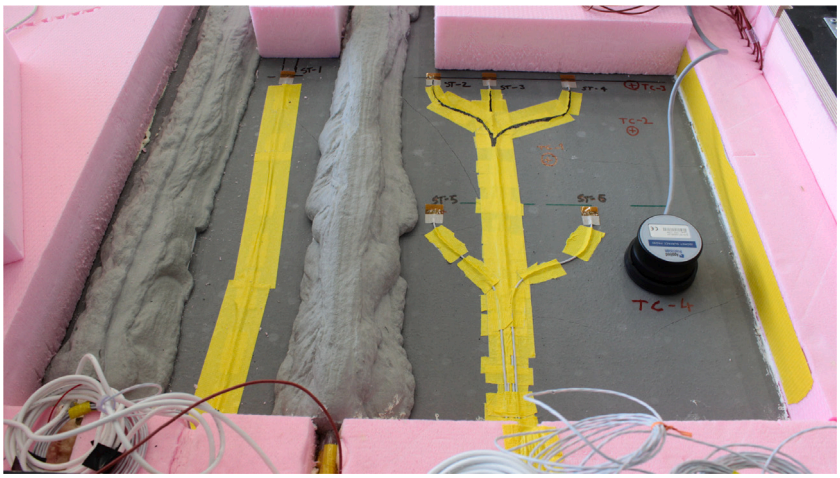

Fig. 12. Top of the concrete panel showing the surface temperature sensors before the top insulation layer was applied.

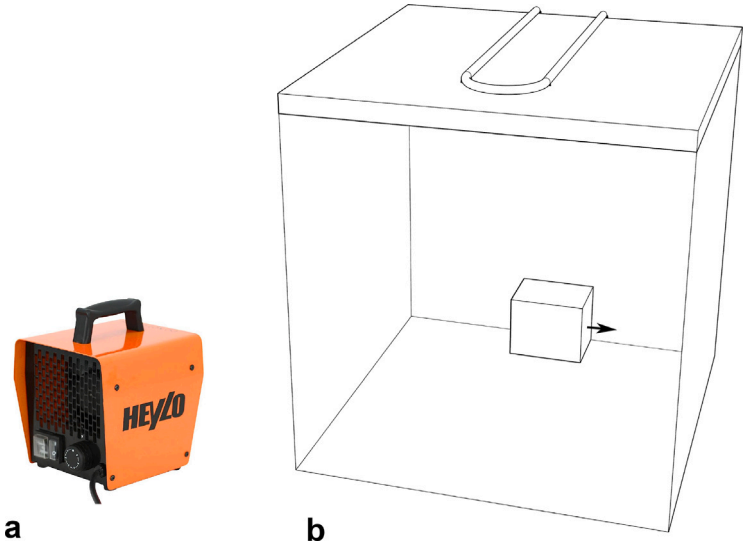

Fig. 13. Heater for internal heat load. (a) Image of the electric heater type: Heylo DE 2XL 2 kW (168 mm × 223 mm × 185 mm). (b) Schematic of the climate chamber showing the location of the heater with the airflow direction.

Table 3
Experiment plan II.

Experiment		Electric heater state	Electric fan state	Electric heater set point [°C]	Chamber door state	Duration [h]
Case	Type					
10	Passive cooling	On	On	45	Closed	4

For TABS heating, Fig. 14 shows the results for Case 1 with a TABS supply temperature of 30 °C. The sensors are the pole group (CP_0, CP_1, CP_2 and CP_3) that captures air temperature in the chamber, and the surface temperatures of the TABS ceiling surface (TL_1) and the floor surface (CF_0) of the chamber. Collectively, these sensors represent a vertical line at the centre of the chamber. In Fig. 14, the *y*-axis variable is the normalised height of the chamber, and the *x*-axis variable is temperature. The results show a temperature profile with a time step of four hours for a duration of 72 h. This result outlines the dynamic relationship between the lightweight TABS, the internal air and chamber surfaces.

The heating mechanism has a two-step process from the initial temperature of 13 °C to the target comfort conditions (e.g. chamber air temperature of 21 °C), as highlighted in Fig. 14.

Firstly, the active surface approaches its steady state condition. In the first four hours, the surface temperature (TL_1) increases by approximately 10 °C. The time to complete the first step is improved compared to a heavyweight TABS due to the thinness of the concrete panel.

Secondly, the room air and non-active surfaces increase their temperatures in response to the active surface temperature. However, the second step is not directly related to TABS panel thickness, but it is purely related to the physics of a ceiling-level heating system where the convective heat transfer coefficient is less than that of a floor-level system (Table 1). The air temperature (CP_2) increases by approximately 2 °C in the first four hours. This time lag in reaching the planned comfort condition can be mitigated with a control strategy that accounts for the latency. To support control refinement, the results provide an understanding of the time delay, and this insight can be applied to improve thermal comfort and energy efficiency in operation.

For TABS cooling, Fig. 15 shows the results for Case 4 with a TABS supply temperature of approximately 20 °C. The temperature profiles have a time step of four hours for a duration of 24 h. The cooling mode does not have a strongly decoupled mechanism as in the heating mode due to the higher total heat transfer coefficient for ceiling-level cooling (Table 1).

In passive natural ventilation mode, we investigated the change in temperature with time of the thermal mass of the lightweight TABS (concrete panel). The hydronic system was switched off for the total duration of the experiment. The chamber door was removed entirely, and the interior of the climate chamber was exposed to the air conditions of the test room. This natural ventilation setup can be classified as a single-sided opening driven by buoyancy alone (no wind effects). The ventilation rate is defined as the flow rate of air into the climate chamber and can be estimated using the following equation [46]:

$$Q = C_d A \sqrt{\frac{\Delta T g h}{(T_I + 273.15)}} \tag{3}$$

where Q is the ventilation rate (m^3/s), C_d is the discharge coefficient, A is the area of the opening (m^2), h is the height of the opening (m), T_I is the internal temperature of the climate chamber (°C), Δ T is the temperature difference between the test room and climate chamber (°C) and g is the gravitational force per unit mass (m/s^2).

Fig. 16 shows the temperature profiles for Case 7 with a time step of four hours for a duration of 24 h. Due to the relatively high ventilation rate, intermediate time steps of one hour are also plotted for the initial 4 h of the experiment.

The results indicate that the lightweight materials (wood) of the floor have a faster cooling rate when compared to the heavy materials (concrete) of the ceiling. After one hour, the ceiling surface sensor (TL_1) shows a temperature change of 0.5 °C, while the floor sensor (CF_1) shows a temperature change of 2.9 °C (Fig. 16). This difference is due to the lower heat capacity of the wood and the lower temperature of the ventilating air stream, which interacts first with the floor surface due to buoyancy forces. This outcome highlights the advantages of including a natural ventilation strategy with the lightweight TABS concept. Ideally, a night flushing approach could be applied to pre-cool buildings with office usage. Further work is required to quantify the full-scale benefit with a reduced ventilation flow rate.

4.2. Reaction time of the lightweight TABS

In active heating mode, we investigated the reaction time for the lightweight TABS for a range of supply temperatures. Fig. 17 shows the results for TABS supply temperatures of 30 °C (Case 1), 35 °C (Case 2) and 40 °C (Case 3). The sensors are from the TABS panel group that provides the temperature at the upper (TU_1) and lower surface (TL_1) of the TABS panel. It should be noted that there are differences in initial conditions for the three cases due to slight variations in starting temperature for each experiment.

Table 4 shows the heat transfer rate from the TABS to the climate chamber (TABS power) for Cases 1, 2 and 3. For each case, the mean values of each parameter are provided over two 24-hour periods during the experiments. All data was collected from the Belimo device. The measured values were supply water temperature, return water temperature and volumetric flow rate. The TABS power (q (W)) was calculated by the Belimo device using the following equation:

$$q = c_p \rho \dot{V} \Delta T \tag{4}$$

where c_p is the specific heat capacity of the TABS fluid (J/kg K), ρ is the density of the TABS fluid (kg/m^3), Δ T is the temperature difference between the supply and return temperature (K) and $\dot{V}$ is the volumetric flow rate (m^3/s) of the TABS fluid.

4.3. Thermal mass and natural ventilation

In passive natural ventilation mode, we studied the change in temperature with time of the thermal mass of the lightweight TABS (concrete panel). Fig. 18 shows the results for Case 7. The sensors are from the TABS group that provides the temperature at the upper (TU_1) and lower surface (TL_1) of the TABS panel. The internal chamber (CP_3) and the test room (external) air temperatures (CWE_0) are also plotted.

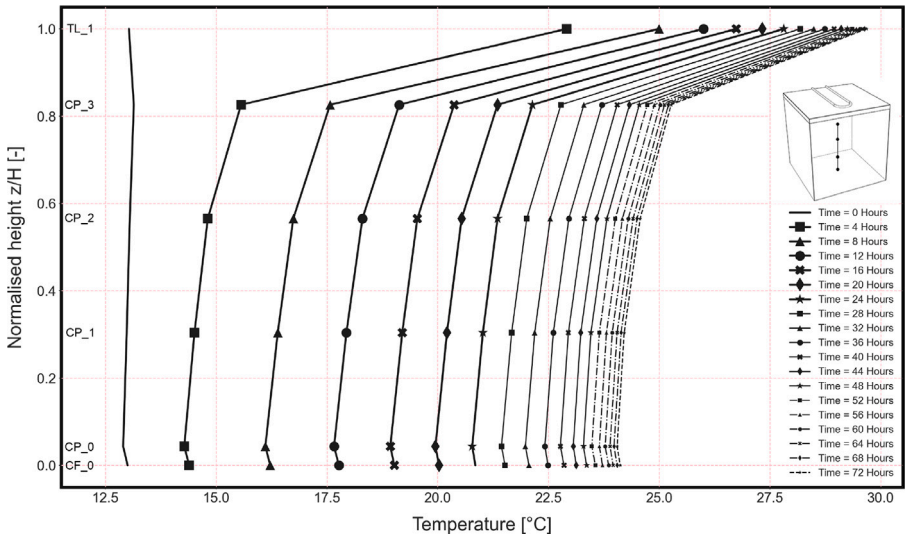

Fig. 14. Heating mode — Relationship between TABS supply temperature and the temperature of the air in the climate chamber. Results from experiment Case 1 (30 °C). Surface (CF_0 and TL_1) and air (CP_0, CP_1, CP_2 and CP_3) temperature measurements showing the dynamic temperature profile (time step = 4 h) in the climate chamber.

Table 4
Hydronic sensors. All values from the Belimo device are averaged over a 24 h time period.

Experiment		TABS				
Case	Period	Supply temperature [°C]	Return temperature [°C]	Temperature difference [°C]	Flow rate [l/min]	Power [W]
1	a	30.86	30.60	0.27	4.10	75.95
	b	30.83	30.57	0.26	4.08	72.83
2	a	35.70	35.39	0.31	4.07	88.37
	b	35.69	35.39	0.30	4.07	83.70
3	a	40.50	40.18	0.33	4.05	91.19
	b	40.48	40.17	0.32	4.03	90.18

4.4. Thermal mass and internal thermal load

In passive cooling mode, we examined the change in temperature with time of the thermal mass of the lightweight TABS (Table 3). An electrical resistance heater (2 kW) with an integrated fan represented the internal heat load. The fan heater was placed inside the climate chamber and controlled using a timer. When the timer was in the 'on' condition, the fan operated continuously, and the heater operated with a temperature set point of 45 °C. Fig. 19a shows the TABS panel's temperature at the upper (TU_1) and lower surface (TL_1). Fig. 19b shows the changes in air temperature of the internal chamber (CP_3) and the external chamber (CWE_0). The fan and the heater's state vectors are shown in Fig. 19c and 19d, respectively. Note that the lower surface sensor is fixed on the lower TABS surface and exposed to the chamber air.

During the loading phase, there is a small temperature difference between the upper (TU_1) and lower (TL_1) surfaces of the TABS (Fig. 19a). This feature indicates that the concrete panel has reached its heat capacity, and the overall panel temperature continues to rise. This result suggests that the panel thinness reduces the storage capacity but retains a useful passive heat storage feature. It should be noted that the internal thermal load (2 kW) is relatively high compared to the heat source for the active heating cases (Table 4).

5. Discussion and future work

5.1. Lifecycle energy design

Pressures to reduce the overall lifecycle energy of a building encourage the use of materials with lower embodied energy [47]. This strategy could include the use of wood for the building structure. Replacing reinforced concrete with structural timber can reduce GHG emissions during the initial phase of a building's lifecycle [48]. However, the thermal properties of wood are not ideal for integrating renewable energy sources in buildings [49] due to a mismatch in thermal proprieties (e.g. thermal conductivity) and the reliance on large surface areas for heat emission.

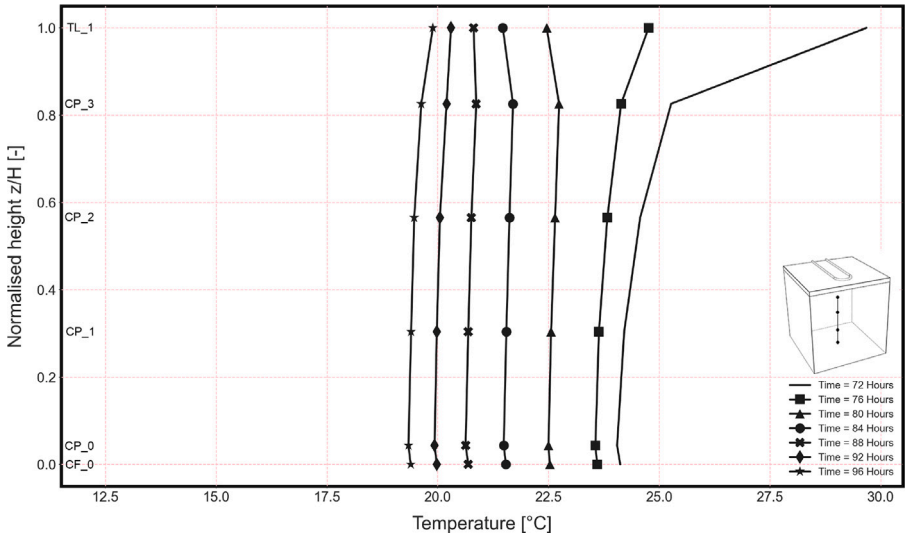

Fig. 15. Cooling mode — Relationship between TABS supply temperature and the temperature of the air in the climate chamber. Results from experiment Case 4. Surface (CF_0 and TL_1) and air (CP_0, CP_1, CP_2 and CP_3) temperature measurements showing the dynamic temperature profile (time step = 4 h) in the climate chamber.

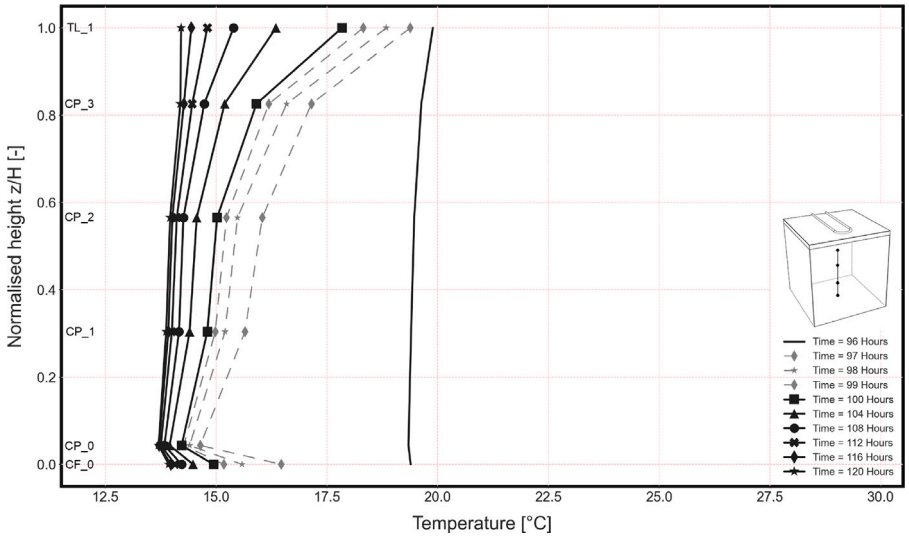

Fig. 16. Natural ventilation mode — Relationship between the temperature of the air and surfaces in the climate chamber (internal) and the temperature of the air in the test room (external). Results from experiment Case 7. Surface (CF_0 and TL_1) and air (CP_0, CP_1, CP_2 and CP_3) temperature measurements showing the dynamic temperature profile (time step = 4 h) in the climate chamber.

Our results indicate that selecting a combination of materials based on function (e.g. structural, thermal) can positively impact embodied and operational energy usage. This approach recognises that materials selection can significantly impact operational energy performance.

For example, the climate chamber is mainly composed of wooden construction. However, the lightweight TABS at the ceiling level retains sufficient thermal storage capabilities to support the efficient operation of TABS. These thermal properties are vital to the adaptation of low-temperature conditioning systems with a renewable source. Further, the surfaces of wooden materials at the floor level have a faster cooling rate when compared to the heavy materials (e.g. concrete) of the ceiling. This feature can be utilised to incorporate natural ventilation strategies. These results highlight the importance of integrated design approaches that consider the potential of synergies from multidisciplinary collaboration.

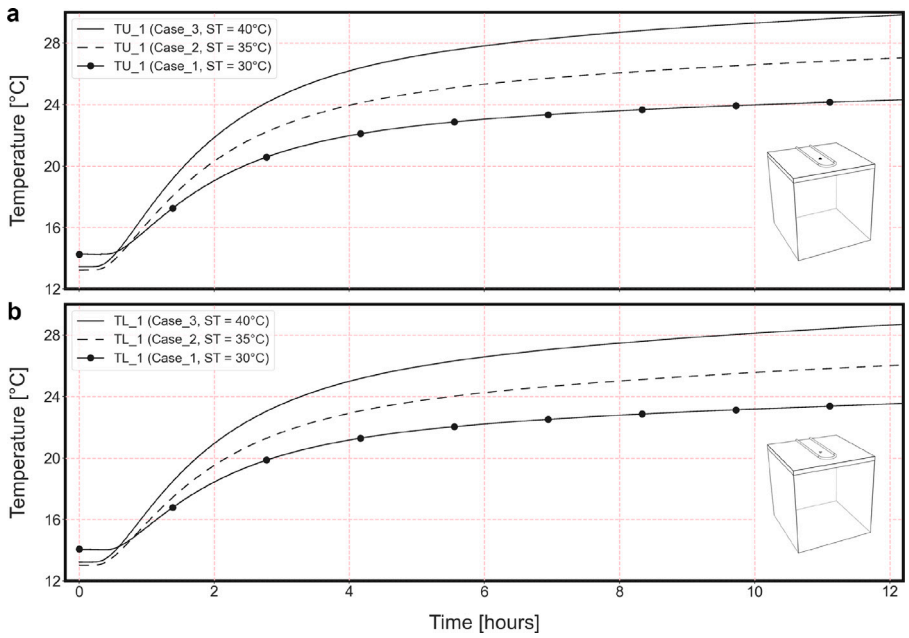

Fig. 17. Heating mode — Reaction time of lightweight TABS. Results from Case: 1, 2 and 3. (a) Temperature of the upper surface (TU_1) of the TABS panel for a range of supply temperatures. (b) Temperature of the lower surface (TL_1) of the TABS panel for a range of supply temperatures (30 °C, 35 °C and 40 °C).

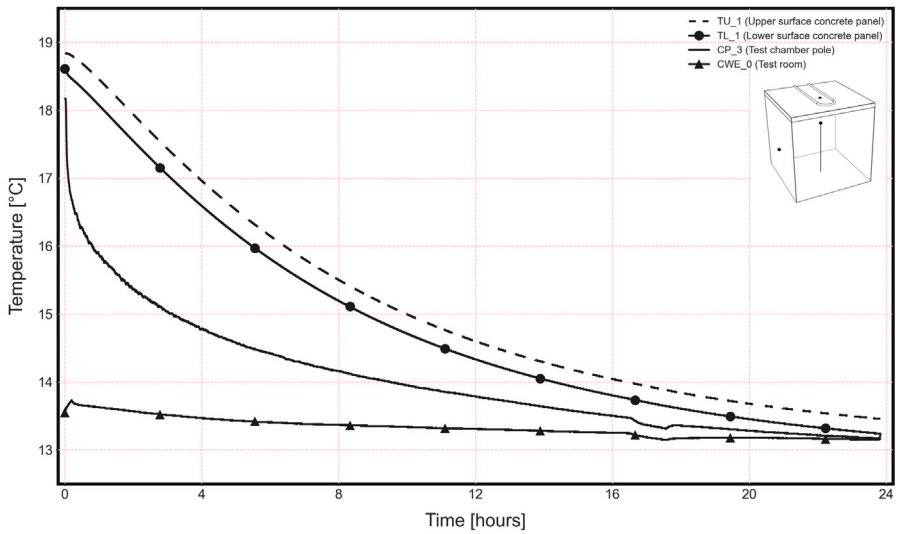

Fig. 18. Natural ventilation mode — Thermal behaviour of the concrete panel. Results from experiment Case 7. Temperature of the upper surface (TU_1) and lower surface (TL_1) of the TABS panel related to climate chamber (CP_3) and test room (CWE_0) temperature.

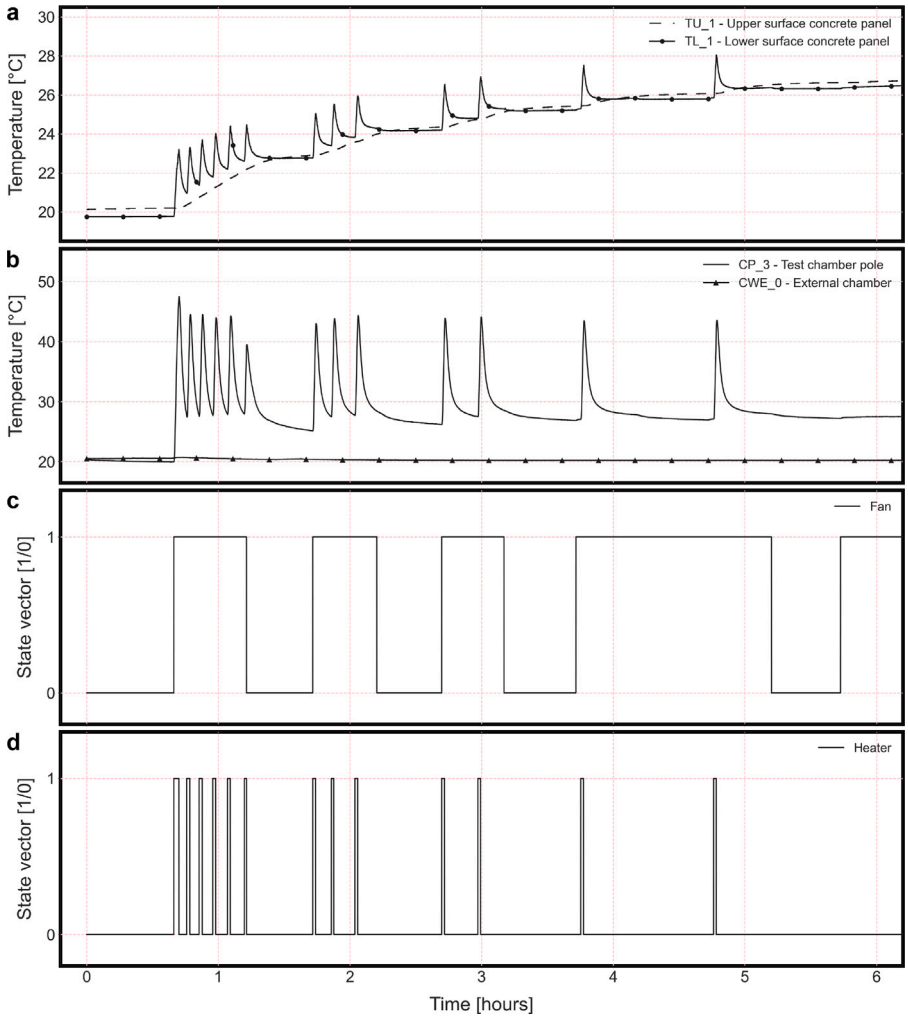

Fig. 19. Passive cooling mode — Thermal behaviour of the concrete panel. Results from experiment Case 10. (a) Temperature of the upper surface (TU_1) and lower surface (TL_1) of the concrete panel. (b) Temperature of the climate chamber (CP_3) and test room (CWE_0). The state vectors of (c) the fan and (d) the heater are also plotted.

5.2. Response time of lightweight TABS

The slow response time of TABS is often cited as a problem for the adoption of low-temperature conditioning methods [50,51]. This response time can be viewed as a two-step mechanism.

The first step relates to the time the active surface takes to converge on its steady state condition in reply to the temperature of the circulating fluid. Our results show that the time to complete this step can be improved with lightweight TABS. The second step relates to the reaction of the non-active surfaces and room air to the surface temperature of the active panel. The thinness of the active panel does not directly influence the second step, and it is primarily related to the heat transfer mode and the location of the active surface. There can be a significant time lag associated with the second step for the heating case at the ceiling level due to the low convective heat transfer coefficient.

One approach to further reduce the time lag of the second step is to couple the room ventilation system with the radiant panel [31], improving the convective heat transfer coefficient in heating mode. Further, this integration has the potential to enhance the mixing of air within the room.

5.3. Small-scale to full-scale experiments

The small-scale experiment supported the development of the lightweight TABS concept. The key benefit was a detailed examination of the dynamic performance of a lightweight TABS panel, which is more difficult on full-scale measurements in a real building due to disturbances (e.g. occupants) and system complexity (e.g. simultaneous operation of HVAC systems). The results

were used to validate high-resolution models and support the design of a full-scale demonstrator. The validated model also supported the quantification the differences between light and heavyweight systems.

In future work, a detailed analysis of the validated model will be presented. Further, the impact of scaling up the models based on the climate chamber measurement will be compared to further studies from the full-scale demonstrator. Thermal response indicators (e.g. HTE and HSE) will be used during this phase due to the complexity of the TABS geometry. In addition, further research on the impact of radiative heat transfer between the surfaces of lightweight and heavy weight materials would be beneficial.

The small-scale experiment made a valuable contribution to the early development of the lightweight TABS. However, the next project steps will be focused on documenting the construction of the full-scale demonstrator and testing the operational performance of the installed systems. The combination of the measurements on both scales will deepen the understanding of the performance of the systems.

6. Conclusion

A small-scale climate chamber with a prototype of lightweight TABS at ceiling level was considered in this study. The work investigated the relationship between the supply temperature of a lightweight TABS and the climate chamber's internal air temperature for active heating, cooling, and natural ventilation modes. A summary of the main conclusions is provided below:

- The reaction time of the TABS has a two-step mechanism. For the first step, our results indicate that the active panel's thinness can improve the reaction time in achieving the target surface temperature of the lightweight TABS. The feature is valid for heating and cooling modes.
- The second step relates to the time lag between achieving the target temperature of the active panel and comfortable conditions in the chamber. This step is not directly influenced by panel thickness. This feature is pronounced in heating mode due to the convective heat transfer coefficient at ceiling level.
- The reaction time relating to the second step could be improved by integrating the ventilation system with the lightweight TABS. This change is associated with an increased convective heat transfer coefficient at the active panel surface.
- A mixture of high and low embodied energy materials within a building zone could positively impact operational energy. For example, concrete at the ceiling level is used to embed the TABS and supplies compatible thermal storage properties. At floor level, the low embodied energy material has a faster surface cooling rate due to the thermal properties of wood. This feature can be combined with a natural ventilation strategy.
- The thinness of the concrete panel reduces the passive thermal storage capacity of the lightweight TABS. However, the remaining thermal storage properties are still relevant for passive cooling.

The results provide experimental data, which can be used to validate high-resolution numerical models. These models can be applied to advance lightweight structural elements to utilise renewable thermal energy for heating and cooling buildings.

CRediT authorship contribution statement

G.P. Lydon: Conceptualization, Methodology, Investigation, Validation, Formal analysis, Data curation, Visualization, Writing – original draft. **A. Schlueter:** Writing – review & editing, Supervision, Project administration.

Declaration of competing interest

The authors declare that they have no known competing financial interests or personal relationships that could have appeared to influence the work reported in this paper.

Data availability

Experimental data will be made available on request.

Acknowledgement

This research was supported by the National Centre of Competence in Research (NCCR) Digital Fabrication, which is funded by the Swiss National Science Foundation.

Appendix A. Climate chamber construction

See Tables 5 and 6.

Table 5
Climate chamber materials.

Component	Material layer	Density kg/m^3	Specific heat capacity J/(kg K)	Thermal conductivity W/m K	Layer thickness m
Walls and floor	Plywood	700	1600	0.17	0.018
	XPS insulation	30	1450	0.035	0.08
	XPS insulation	30	1450	0.035	0.08
	Plywood	700	1600	0.17	0.018
Door	Plywood	700	1600	0.17	0.018
	XPS insulation	30	1450	0.035	0.08
	XPS insulation	30	1450	0.035	0.08
	Plywood	700	1600	0.17	0.018
Ceiling (Active)	XPS insulation	30	1450	0.035	0.08
	XPS insulation	30	1450	0.035	0.08
	Concrete cover	1350	1000	0.82	0.03
	Concrete	1800	1000	1.4	0.035

Table 6
Data point list.

Group	Label	Location	Parameter	Unit	Sensor	Accuracy	Range	Manufacturer
Floor	CF_0	Floor surface	Temperature	°C	PT100	±0.3 °C at 0 °C	−50 °C to +200 °C	Sensoren
sensors	CF_1	Floor surface	Temperature	°C	PT100	±0.3 °C at 0 °C	−50 °C to +200 °C	Sensoren
	CF_2	Floor surface	Temperature	°C	PT100	±0.3 °C at 0 °C	−50 °C to +200 °C	Sensoren
	CF_3	Floor surface	Temperature	°C	PT100	±0.3 °C at 0 °C	−50 °C to +200 °C	Sensoren
Wall	CW_0	Wall surface	Temperature	°C	PT100	±0.3 °C at 0 °C	−50 °C to +200 °C	Sensoren
sensors	CW_1	Wall surface	Temperature	°C	PT100	±0.3 °C at 0 °C	−50 °C to +200 °C	Sensoren
	CW_2	Wall surface	Temperature	°C	PT100	±0.3 °C at 0 °C	−50 °C to +200 °C	Sensoren
	CW_3	Wall surface	Temperature	°C	PT100	±0.3 °C at 0 °C	−50 °C to +200 °C	Sensoren
Pole	CP_0	Pole	Temperature	°C	PT1000	±0.03 °C at 0 °C	−50 °C to +200 °C	Sensoren
sensors	CP_1	Pole	Temperature	°C	PT1000	±0.03 °C at 0 °C	−50 °C to +200 °C	Sensoren
	CP_2	Pole	Temperature	°C	PT1000	±0.03 °C at 0 °C	−50 °C to +200 °C	Sensoren
	CP_3	Pole	Temperature	°C	PT1000	±0.03 °C at 0 °C	−50 °C to +200 °C	Sensoren
TABS	TL_1	Lower surface	Temperature	°C	PT100	±0.3 °C at 0 °C	−73 to 260 °C	Omega Engineering
sensors	TL_2	Lower surface	Temperature	°C	PT100	±0.3 °C at 0 °C	−73 to 260 °C	Omega Engineering
	TL_5	Lower surface	Temperature	°C	PT100	±0.3 °C at 0 °C	−73 to 260 °C	Omega Engineering
	TU_1	Upper surface	Temperature	°C	PT100	±0.3 °C at 0 °C	−73 to 260 °C	Omega Engineering
	TU_2	Upper surface	Temperature	°C	PT100	±0.3 °C at 0 °C	−73 to 260 °C	Omega Engineering
	TU_3	Upper surface	Temperature	°C	PT100	±0.3 °C at 0 °C	−73 to 260 °C	Omega Engineering
	TU_4	Upper surface	Temperature	°C	PT100	±0.3 °C at 0 °C	−73 to 260 °C	Omega Engineering
	TP_0	Pipe	Temperature	°C	PT100	±0.3 °C at 0 °C	−50 °C to +200 °C	Sensoren
Hydronic	WS_0	Supply line	Temperature	°C	PT1000	±0.35 °C at 10 °C	−20 °C to +80 °C	Belimo
sensors	WS_1	Supply line	Flow rate	l/min	Ultrasonic	±2% at 20 °C	–	Belimo
	WS_2	Pump control	Temperature	%	–	±5% at 20 °C	–	Belimo
	WR_0	Return line	Temperature	°C	PT1000	±0.35 °C at 10 °C	−20 °C to +80 °C	Belimo
Test room	RE_1-H	Test room	Relative humidity	%	Digital	±3% r. H. at 20 °C	0 to 95% r.H.	S+S Regeltechnik
sensors	RE_1-T	Test room	Temperature	°C	Digital	±0.2 °C at 25 °C	−35 °C to +75 °C	S+S Regeltechnik
	CWE_0	Boundary wall	Temperature	°C	PT100	±0.3 °C at 0 °C	−50 °C to +200 °C	Sensoren
	CFE_0	Boundary floor	Temperature	°C	PT100	±0.3 °C at 0 °C	−50 °C to +200 °C	Sensoren

Appendix B. Result plots

See Figs. 20–22.

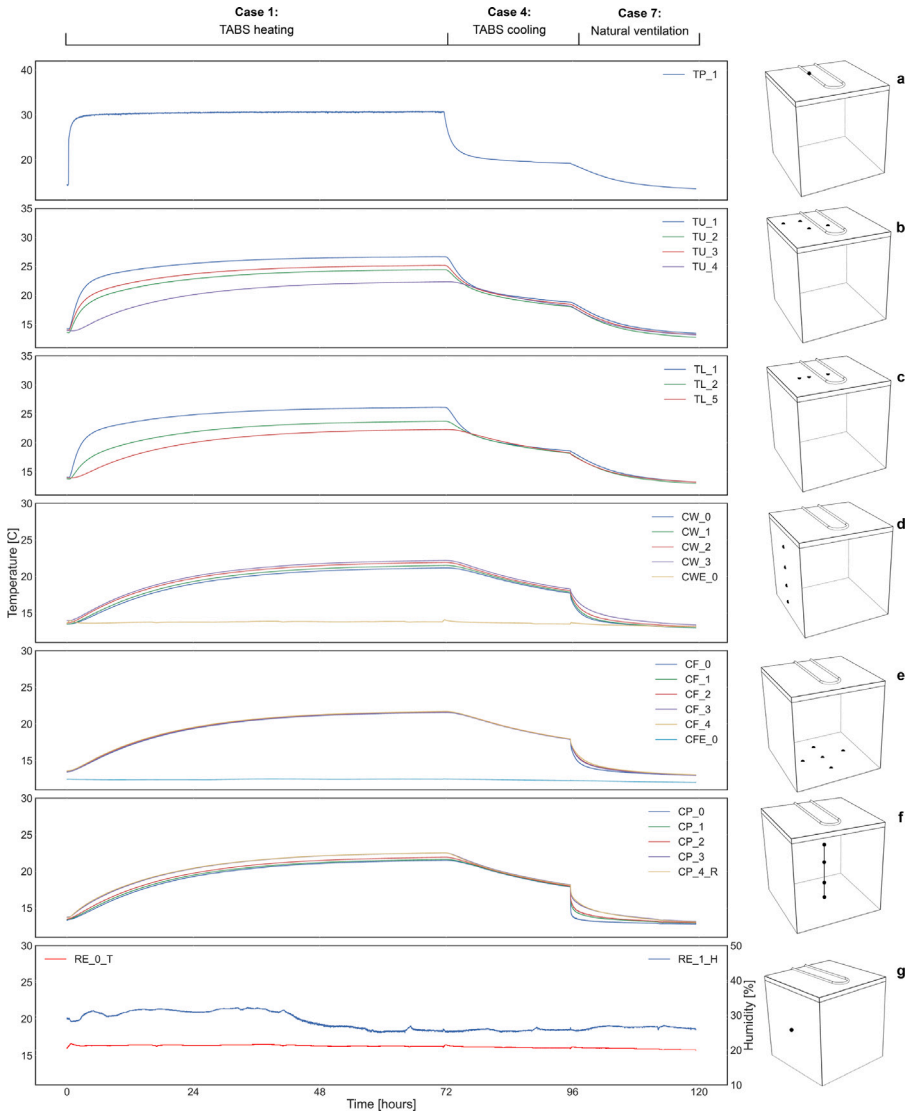

Fig. 20. Results from experiments 1, 4 and 7. (a) Embedded temperature sensor on the TABS pipework. (b) TABS panel sensor group on the upper surface. (c) TABS panel sensor group on the lower surface. (d) Chamber wall sensor group. (e) Chamber floor sensor group. (f) Chamber pole sensor group. (g) External room sensor group.

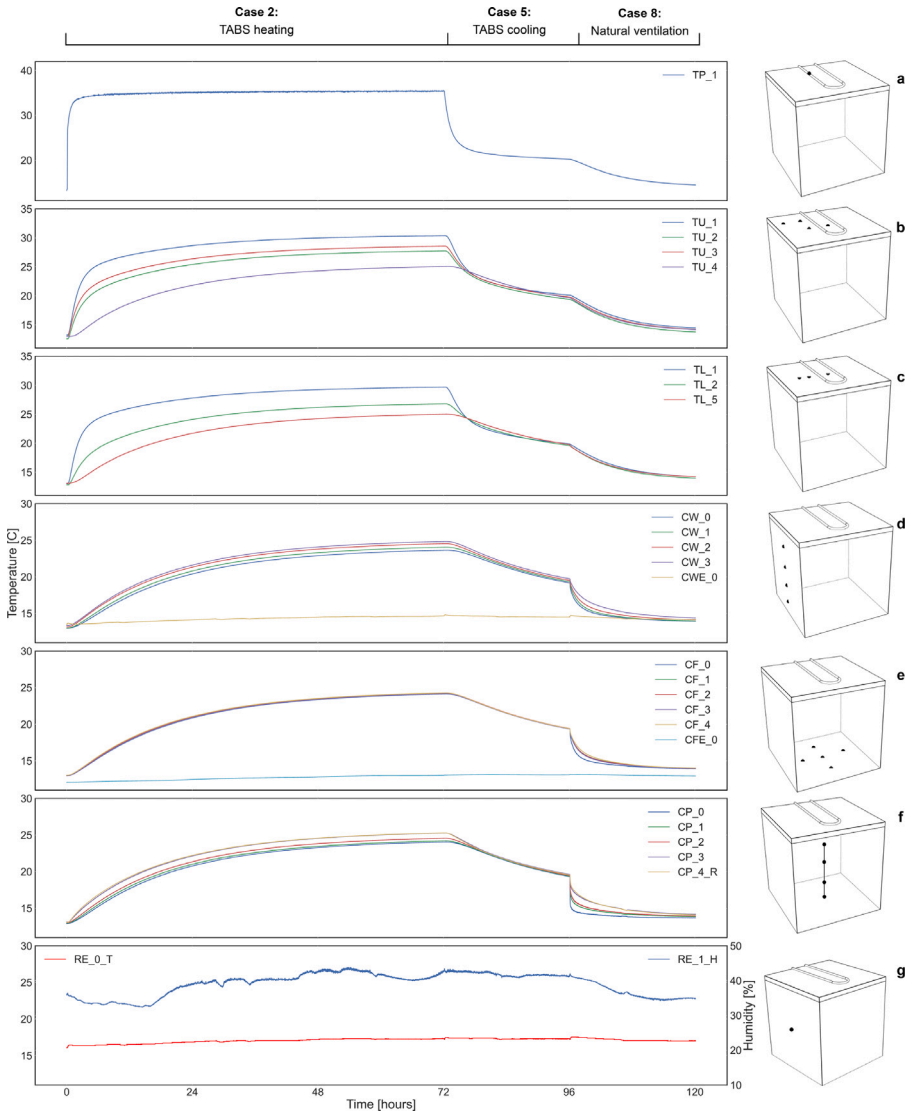

Fig. 21. Results from experiments 2, 5 and 8. (a) Embedded temperature sensor on the TABS pipework. (b) TABS panel sensor group on the upper surface. (c) TABS panel sensor group on the lower surface. (d) Chamber wall sensor group. (e) Chamber floor sensor group. (f) Chamber pole sensor group. (g) External room sensor group.

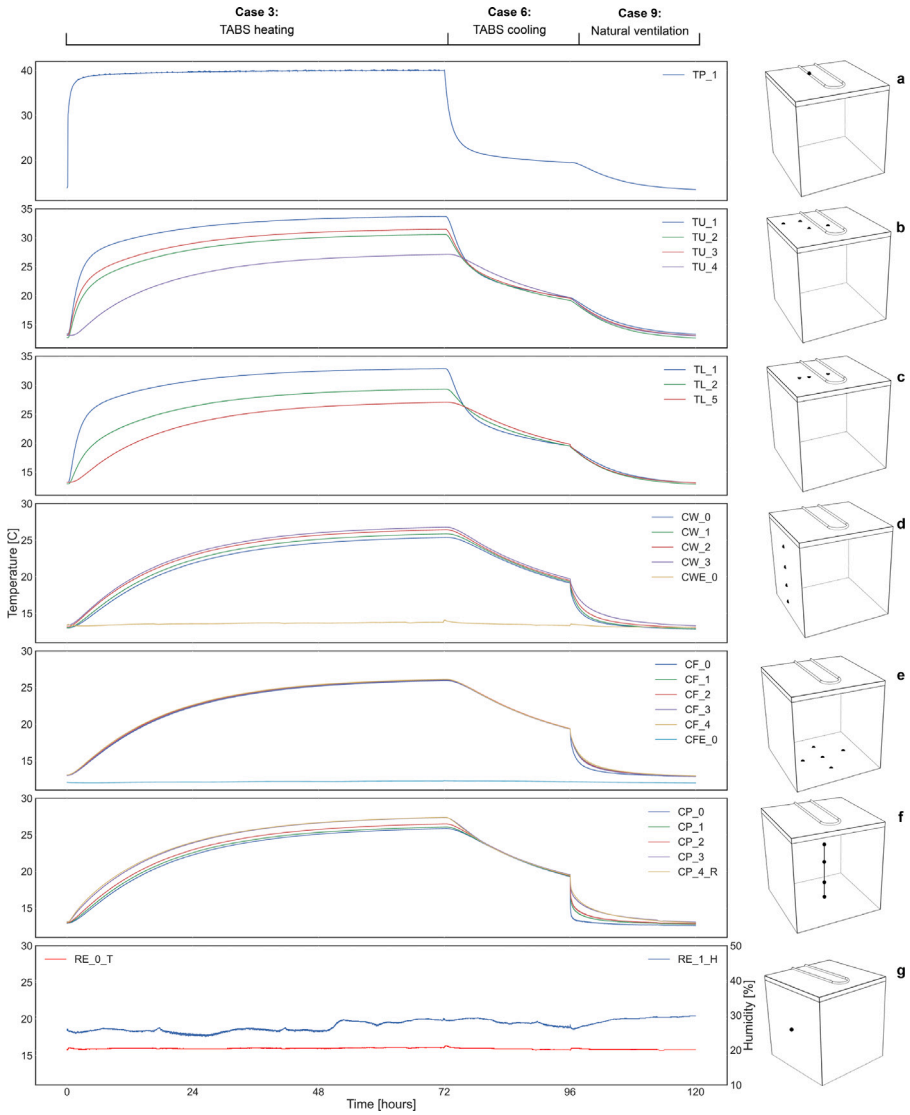

Fig. 22. Results from experiments 3, 6 and 9. (a) Embedded temperature sensor on the TABS pipework. (b) TABS panel sensor group on the upper surface. (c) TABS panel sensor group on the lower surface. (d) Chamber wall sensor group. (e) Chamber floor sensor group. (f) Chamber pole sensor group. (g) External room sensor group.

References

[1] B. Lehmann, V. Dorer, M. Koschenz, Application range of thermally activated building systems tabs, Energy Build. 39 (5) (2007) 593–598, http://dx.doi.org/10.1016/j.enbuild.2006.09.009.

[2] D. Schmidt, Low exergy systems for high-performance buildings and communities, Energy Build. 41 (3) (2009) 331–336, http://dx.doi.org/10.1016/j.enbuild.2008.10.005.

[3] A. Allen, G. Henze, K. Baker, G. Pavlak, Evaluation of low-exergy heating and cooling systems and topology optimization for deep energy savings at the urban district level, Energy Convers. Manage. 222 (2020) 113106, http://dx.doi.org/10.1016/j.enconman.2020.113106.

[4] H.E. Feustel, C. Stetiu, Hydronic radiant cooling — preliminary assessment, Energy Build. 22 (3) (1995) 193–205, http://dx.doi.org/10.1016/0378-7788(95)00922-K.

[5] S.P. Corgnati, A. Kindinis, Thermal mass activation by hollow core slab coupled with night ventilation to reduce summer cooling loads, Build. Environ. 42 (9) (2007) 3285–3297, http://dx.doi.org/10.1016/j.buildenv.2006.08.018.

[6] D. Rijksen, C. Wisse, A. van Schijndel, Reducing peak requirements for cooling by using thermally activated building systems, Energy Build. 42 (3) (2010) 298–304, http://dx.doi.org/10.1016/j.enbuild.2009.09.007.

[7] P. Busch, A. Kendall, C.W. Murphy, S.A. Miller, Literature review on policies to mitigate GHG emissions for cement and concrete, Resour. Conserv. Recy. 182 (2022) 106278, http://dx.doi.org/10.1016/j.resconrec.2022.106278.

[8] J. Goggins, T. Keane, A. Kelly, The assessment of embodied energy in typical reinforced concrete building structures in Ireland, Energy Build. 42 (5) (2010) 735–744, http://dx.doi.org/10.1016/j.enbuild.2009.11.013.

[9] B. Yan, X. Han, A. Malkawi, T.H. Dokka, P. Howard, J. Knowles, T. Hegli, K. Edwards, Comprehensive assessment of operational performance of coupled natural ventilation and thermally active building system via an extensive sensor network, Energy Build. 260 (2022) 111921, http://dx.doi.org/10.1016/j.enbuild.2022.111921.

[10] G. Lydon, A. Willmann, J. Hofer, Z. Nagy, A. Schlueter, Balancing operational and embodied emissions for the energy concept of an experimental research and living unit, in: CISBAT, Lausanne, Switzerland, 2015.

[11] G. Lydon, J. Hischier, A. Schlueter, High-resolution analysis for the development of TABS in lightweight structures, in: IBPSA Building Simulation 2017, San Francisco, USA, 2017.

[12] D. López López, D. Veenendaal, M. Akbarzadeh, P. Block, Prototype of an ultra-thin, concrete vaulted floor system, in: Proceedings of the IASS-SLTE 2014 Symposium, Brasilia, Brazil, 2014.

[13] P. Block, Thrust Network Analysis: Exploring Three-dimensional Analysis (Ph.D. thesis), Massachusetts Institute of Technology, Cambridge, MA, USA, 2009.

[14] G. Lydon, J. Hofer, B. Svetozarevic, Z. Nagy, A. Schlueter, Coupling energy systems with lightweight structures for a net plus energy building, Appl. Energy 189 (2017) 310–326, http://dx.doi.org/10.1016/j.apenergy.2016.11.110.

[15] A. Jipa, C.C. Barentin, G. Lydon, M. Rippmann, G. Chousou, M. Lomaglio, A. Schlueter, P. Block, B. Dillenburger, 3D-printed formwork for integrated funicular concrete slabs, in: Proceedings of IASS Annual Symposia, vol. 2019, (6) 2019, pp. 1–8.

[16] G. Lydon, S. Caranovic, I. Hischier, A. Schlueter, Coupled simulation of thermally active building systems to support a digital twin, Energy Build. 202 (2019) 109298, http://dx.doi.org/10.1016/j.enbuild.2019.07.015.

[17] G. Lydon, J. Hofer, Z. Nagy, A. Schlueter, Thermal analysis of a multifunctional floor element, in: Third IBSPA Building Simulation & Optimisation, Newcastle, England, 2016.

[18] M. Sharifi, I.C. Figueroa, R. Mahmoud, E. Himpe, L. Helsen, J. Laverge, Early-stage optimal design of hybrid GEOTABS buildings in terms of costs and CO2 emissions, Energy Convers. Manage. 257 (2022) 115392, http://dx.doi.org/10.1016/j.enconman.2022.115392.

[19] B.W. Olesen, F. Bonnefoi, E. Michel, M.d. Carli, Heat exchange coefficient between floor surface and space by floor cooling – theory or a question of definition, 2000.

[20] Y. Li, M. Sandberg, L. Fuchs, Effects of thermal radiation on airflow with displacement ventilation: an experimental investigation, Energy Build. 19 (4) (1993) 263–274, http://dx.doi.org/10.1016/0378-7788(93)90011-I.

[21] S. Gilani, H. Montazeri, B. Blocken, CFD simulation of stratified indoor environment in displacement ventilation: Validation and sensitivity analysis, Build. Environ. 95 (2016) 299–313, http://dx.doi.org/10.1016/j.buildenv.2015.09.010.

[22] J. Babiak, B. Olesen, D. Petras, Low Temperature Heating and High Temperature Cooling: REHVA GUIDEBOOK No 7, REHVA, 2007.

[23] J. Shinoda, O.B. Kazanci, S. ichi Tanabe, B.W. Olesen, A review of the surface heat transfer coefficients of radiant heating and cooling systems, Build. Environ. 159 (2019) 106156, http://dx.doi.org/10.1016/j.buildenv.2019.05.034.

[24] M. Krajčík, M. Arıcı, O. Šikula, M. Šimko, Review of water-based wall systems: Heating, cooling, and thermal barriers, Energy Build. 253 (2021) 111476, http://dx.doi.org/10.1016/j.enbuild.2021.111476.

[25] M. Berger, J. Worlitschek, The link between climate and thermal energy demand on national level: A case study on Switzerland, Energy Build. 202 (2019) 109372, http://dx.doi.org/10.1016/j.enbuild.2019.109372.

[26] F.M. Amoruso, T. Schuetze, Hybrid timber-based systems for low-carbon, deep renovation of aged buildings: Three exemplary buildings in the Republic of Korea, Build. Environ. 214 (2022) 108889, http://dx.doi.org/10.1016/j.buildenv.2022.108889.

[27] I. ISO, 11855-6: Building environment design–design, dimensioning, installation and control of embedded radiant heating and cooling systems–Part 6: Control, International Organization for Standardization, Geneva, Switzerland, 2012.

[28] F. Causone, S.P. Corgnati, M. Filippi, B.W. Olesen, Experimental evaluation of heat transfer coefficients between radiant ceiling and room, Energy Build. 41 (6) (2009) 622–628, http://dx.doi.org/10.1016/j.enbuild.2009.01.004.

[29] M. Andrés-Chicote, A. Tejero-González, E. Velasco-Gómez, F.J. Rey-Martínez, Experimental study on the cooling capacity of a radiant cooled ceiling system, Energy Build. 54 (2012) 207–214, http://dx.doi.org/10.1016/j.enbuild.2012.07.043.

[30] M. Krajčík, M. Šimko, O. Šikula, D. Szabó, D. Petráš, Thermal performance of a radiant wall heating and cooling system with pipes attached to thermally insulating bricks, Energy Build. 246 (2021) 111122, http://dx.doi.org/10.1016/j.enbuild.2021.111122.

[31] S. Venko, E. Pavlovič, B. Vidrih, C. Arkar, S. Medved, An experimental study of mixed convection over various thermal activation lengths of vertical TABS, Energy Build. 98 (2015) 151–160, http://dx.doi.org/10.1016/j.enbuild.2014.08.036, Renewable Energy Sources and Healthy Buildings.

[32] M. Krajčík, O. Šikula, Heat storage efficiency and effective thermal output: Indicators of thermal response and output of radiant heating and cooling systems, Energy Build. 229 (2020) 110524, http://dx.doi.org/10.1016/j.enbuild.2020.110524.

[33] K. Zhao, X.-H. Liu, Y. Jiang, Dynamic performance of water-based radiant floors during start-up and high-intensity solar radiation, Sol. Energy 101 (2014) 232–244, http://dx.doi.org/10.1016/j.solener.2013.12.033.

[34] M. Krajčík, O. Šikula, The possibilities and limitations of using radiant wall cooling in new and retrofitted existing buildings, Appl. Therm. Eng. 164 (2020) 114490, http://dx.doi.org/10.1016/j.applthermaleng.2019.114490.

[35] L.M. Domínguez, O.B. Kazanci, N. Rage, B.W. Olesen, Experimental and numerical study of the effects of acoustic sound absorbers on the cooling performance of Thermally Active Building Systems, Build. Environ. 116 (2017) 108–120, http://dx.doi.org/10.1016/j.buildenv.2017.02.009.

[36] P. Nageler, G. Schweiger, M. Pichler, D. Brandl, T. Mach, R. Heimrath, H. Schranzhofer, C. Hochenauer, Validation of dynamic building energy simulation tools based on a real test-box with thermally activated building systems (TABS), Energy Build. 168 (2018) 42–55, http://dx.doi.org/10.1016/j.enbuild.2018.03.025.

[37] T. Weber, G. Jóhannesson, M. Koschenz, B. Lehmann, T. Baumgartner, Validation of a FEM-program (frequency-domain) and a simplified RC-model (time-domain) for thermally activated building component systems (TABS) using measurement data, Energy Build. 37 (7) (2005) 707–724, http://dx.doi.org/10.1016/j.enbuild.2004.10.005.
[38] C. Beji, A. Merabtine, S. Mokraoui, A. Kheiri, J. Kauffmann, N. Bouaziz, Experimental study on the effects of direct sun radiation on the dynamic thermal behavior of a floor-heating system, Sol. Energy 204 (2020) 1–12, http://dx.doi.org/10.1016/j.solener.2020.04.055.
[39] D.-I. Bogatu, O.B. Kazanci, B.W. Olesen, An experimental study of the active cooling performance of a novel radiant ceiling panel containing phase change material (PCM), Energy Build. 243 (2021) 110981, http://dx.doi.org/10.1016/j.enbuild.2021.110981.
[40] C. Zhang, P.K. Heiselberg, M. Pomianowski, T. Yu, R.L. Jensen, Experimental study of diffuse ceiling ventilation coupled with a thermally activated building construction in an office room, Energy Build. 105 (2015) 60–70, http://dx.doi.org/10.1016/j.enbuild.2015.07.048.
[41] T. Yu, P. Heiselberg, B. Lei, M. Pomianowski, C. Zhang, R. Jensen, Experimental investigation of cooling performance of a novel hvac system combining natural ventilation with diffuse ceiling inlet and TABS, Energy Build. 105 (2015) 165–177, http://dx.doi.org/10.1016/j.enbuild.2015.07.039.
[42] M.R. Krusaa, C.A. Hviid, Reduced-scale experiments of heat transfer from integrated radiant ceiling panel and diffuse ceiling ventilation, Appl. Therm. Eng. 197 (2021) 117348, http://dx.doi.org/10.1016/j.applthermaleng.2021.117348.
[43] S. Fohanno, G. Polidori, Modelling of natural convective heat transfer at an internal surface, Energy Build. 38 (5) (2006) 548–553, http://dx.doi.org/10.1016/j.enbuild.2005.09.003.
[44] H. Awbi, A. Hatton, Natural convection from heated room surfaces, Energy Build. 30 (3) (1999) 233–244, http://dx.doi.org/10.1016/S0378-7788(99)00004-3.
[45] J. Shi, J. Tan, B. Liu, Y. Liu, H. Xu, Z. Wang, T. Xiong, J. Shi, Thermal and mechanical properties of thermal energy storage lightweight aggregate mortar incorporated with phase change material, J. Energy Storage 32 (2020) 101719, http://dx.doi.org/10.1016/j.est.2020.101719.
[46] D. Etheridge, Natural Ventilation of Buildings E Theory, Measurement and Design, John Wiley & Sons, Chichester, UK, 2012.
[47] L.F. Cabeza, C. Barreneche, L. Miró, J.M. Morera, E. Bartolí, A. Inés Fernández, Low carbon and low embodied energy materials in buildings: A review, Renew. Sustain. Energy Rev. 23 (2013) 536–542, http://dx.doi.org/10.1016/j.rser.2013.03.017.
[48] J. Nässén, F. Hedenus, S. Karlsson, J. Holmberg, Concrete vs. wood in buildings – An energy system approach, Build. Environ. 51 (2012) 361–369, http://dx.doi.org/10.1016/j.buildenv.2011.11.011.
[49] D. Heidenthaler, M. Leeb, T. Schnabel, H. Huber, Comparative analysis of thermally activated building systems in wooden and concrete structures regarding functionality and energy storage on a simulation-based approach, Energy 233 (2021) 121138, http://dx.doi.org/10.1016/j.energy.2021.121138.
[50] M. Sharifi, R. Mahmoud, E. Himpe, J. Laverge, A heuristic algorithm for optimal load splitting in hybrid thermally activated building systems, J. Build. Eng. 50 (2022) 104160, http://dx.doi.org/10.1016/j.jobe.2022.104160.
[51] M. Mork, A. Xhonneux, D. Müller, Nonlinear distributed model predictive control for multi-zone building energy systems, Energy Build. 264 (2022) 112066, http://dx.doi.org/10.1016/j.enbuild.2022.112066.